High-Temperature Glass Transition in Model C_{60}

Maria C. Abramo, Carlo Caccamo,* Dino Costa, and Romina Ruberto

Istituto Nazionale per la Fisica della Materia (INFM) andDipartimento di Fisica, Università degli Studi di Messina, Contrada Papardo, C.P. 50-98166 Messina, Italy

Received: July 7, 2004; In Final Form: July 29, 2004

C_{60} exhibits a glass transition at 90 K, associated with the quenching of the *orientational* disorder of the fullerene cages. We report evidence from molecular dynamics simulation that a central pair potential model of C_{60} undergoes a glass transition associated with the quenching of *positional* disorder from the liquid phase, at $T_g \simeq 1100$ K for a pressure $P = 3.5$ MPa, and at higher temperatures for higher pressure values. Two remarkable features turn out to be associated with such a basic prediction: the "effective" packing fraction of the system *quantitatively* reproduces that of hard spheres at their own glass transition; a strict analogy emerges between our findings and recent mode coupling theory determinations of structural arrest lines in short-range potential models of protein solutions. We argue on such a basis that the conclusions of the present study hold for a wide class of short-range potentials currently in use to model complex fluids, some of biological interest, this suggesting how to achieve at least qualitative predictions of vitrification in these systems.

It is known that residual orientational disorder of fullerene molecules in the low temperatures fcc crystalline phase of C_{60} can be quenched to form an orientational glass.[1,2] Another glassy phase, associated with positional disorder of C_{60}, might also be formed upon quenching from the (normal or supercooled) liquid phase of this fullerene. Liquid C_{60}, however, has not yet been observed,[3−7] although its existence has been predicted[8−14] for a spherically symmetric pair potential model of C_{60} due to Girifalco.[15] The temperature range of the liquid pocket is rather narrow, the triple and critical point temperature being $T_{tr} \simeq 1880$ K and $T_{cr} \simeq 1940$ K, respectively;[13,14] the liquid is thus "nearly critical" in any case. This characteristic reflects the "marginally" short-range nature of the Girifalco potential and agrees with early speculations about the "elusive diffusive" nature of liquid C_{60},[10] as well as with the absence of cage effects in the velocity autocorrelation functions, and of collective phenomena, ordinarily observed in simple liquids.[16] It also explains the similarity between the phase diagram of the model at issue and that of other complex fluids such as protein solutions or colloidal suspensions wherein, however, the interaction potential is much more short-range than for the C_{60} model, so as to even lead to the disappearance of a stable liquid phase.[8−10,17,18]

Such being the features of model liquid C_{60}, it is not obvious that quenching of its positional disorder can effectively result in a glass transition. As we shall document in this work, this transition does actually take place; the existence of such a glassy phase, of interest per se, is also relevant in the much more general context of complex fluid modeling. In protein solutions, for example, it is known that the success of crystallization procedures is most frequently hampered by the formation of amorphous phases or gels, see e.g. refs 19 and 20 and references therein. Also, in the context of colloid−polymer mixtures, the observation of two glassy states, originating from different structural arrest mechanisms, has been experimentally reported.[21−23] A study of glass transition in the present case might then provide information useful in these and similar systems.

Girifalco's potential reads[15]

$$v(r) = -\alpha_1\left[\frac{1}{s(s-1)^3} + \frac{1}{s(s+1)^3} - \frac{2}{s^4}\right] + \alpha_2\left[\frac{1}{s(s-1)^9} + \frac{1}{s(s+1)^9} - \frac{2}{s^{10}}\right] \quad (1)$$

where $s = r/d$, $\alpha_1 = N^2A/12d^6$, and $\alpha_2 = N^2B/90d^{12}$; N and d are the number of carbon atoms and the diameter, respectively, of the fullerene particles, $A = 32 \times 10^{-60}$ erg cm^6 and $B = 55.77 \times 10^{-105}$ erg cm^{12} are constants entering the 12−6 potential $\phi(r) = -A/r^6 + B/r^{12}$ through which two carbon sites on different spherical molecules are assumed to interact. According to ref 15 $d = 0.71$ nm, whereas the distance at which the potential (1) crosses zero, the position of the potential well minimum, and its depth are $r_0 = 0.959$ nm, $r_{min} = 1.005$ nm, and $\epsilon = 0.444 \times 10^{-12}$ erg, respectively. We assume $v(r) = \infty$ for $s < 1$.

Constant pressure molecular dynamics (MD) have been performed for potential (1) with $N = 864$ and 1000 total number of particles. Note $N = 864$ is fully compatible with a fcc lattice arrangement of the particles while $N = 1000$ implies defects upon crystallization. A time step of 5×10^{-15} s is adopted. Simulations are started from an initial supercritical or liquid configuration (see Figure 1). The cooling is carried out through successive stepwise temperature drops of 30 K, with the system left each time to evolve over 20 000 steps during which the temperature is forced to take the prefixed value, followed by further 10 000 steps over which the system evolves freely and averages are cumulated. The final temperature T, box volume V (or, equivalently, number density of particles ρ), enthalpy H, as well as other thermodynamic, structural, and dynamical properties are recorded at each temperature decrease (see below). Statistical uncertainties on T, ρ, and pressure P are 0.8 K, 0.0003 nm^{-3} and 0.1 MPa, respectively. Most of the reported results refer to $N = 1000$ particles simulations. Calculations with 864 particles essentially reproduce those obtained with 1000 particles.

* To whom correspondence should be addressed. E-mail: carlo.caccamo@unime.it.

10.1021/jp046995f CCC: $27.50
Published on Web 08/13/2004

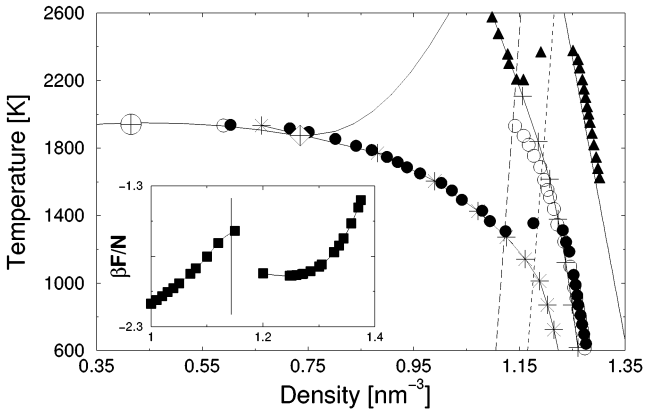

Figure 1. Cooling/quenching and heating paths of model C_{60}. Full lines: liquid−vapor binodal, melting and freezing lines of C_{60}; circle with cross and diamond with cross: critical and triple point, respectively.[14] Full circles (triangles): cooling at 3.5 MPa (250 MPa) with 1000 particles. Line with asterisks (crosses): quenching paths with N = 1000 at P = 3.5 MPa (250 MPa). Open circles: heating of the defective solid with $N = 1000$ at 3.5 MPa. Long-dashed and dashed lines: ρ vs T loci over which $\eta = 0.548$ and 0.574, respectively (see text). Inset: Helmholtz free energy vs ρ at $T = 2100$ K as obtained through simulation in ref 14. The vertical thin line indicates ρ_c(2100 K) = 1.14.

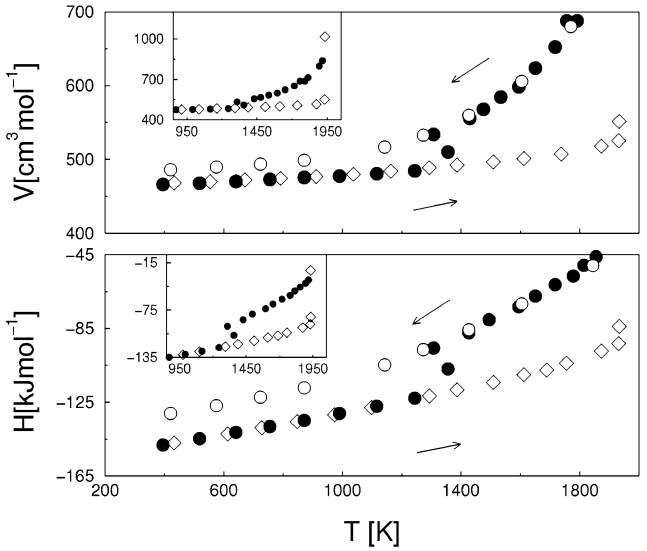

Figure 2. Molar volume (top) and enthalpy (bottom) vs temperature at $P = 3.5$ MPa. Full and open circles: cooling and quenching with $N = 1000$, respectively. Open diamonds: heating of defective solid with $N = 1000$. Insets: cooling and melting of the defective solid documented through an expanded vertical scales.

Cooling paths are visualized in Figure 1 in the $\rho-T$ phase diagram of C_{60}.[13] Volumes and enthalpies at $P = 3.5$ MPa are displayed in Figure 2. As clearly visible, at $T \simeq 1300$ K, both V and H undergo a marked drop, accompanied by a temporary increase of the temperature, in correspondence with the transition to the crystalline (fcc) phase, documented by the behavior of the radial distribution function $g(r)$ for $T \leq 1307$ K shown in Figure 3. The dependence of the diffusion coefficient D on T, also shown in Figure 3, confirms the transition to the solid phase. Cooling cycles with $\Delta T = 15$ K lead to substantially similar results. The crystallization temperature and density, T_c and ρ_c, respectively, are reported in Table 1, also for other pressures investigated. Note that the transition takes place under strong supercooling conditions, well beyond the freezing line and below the triple point temperature.

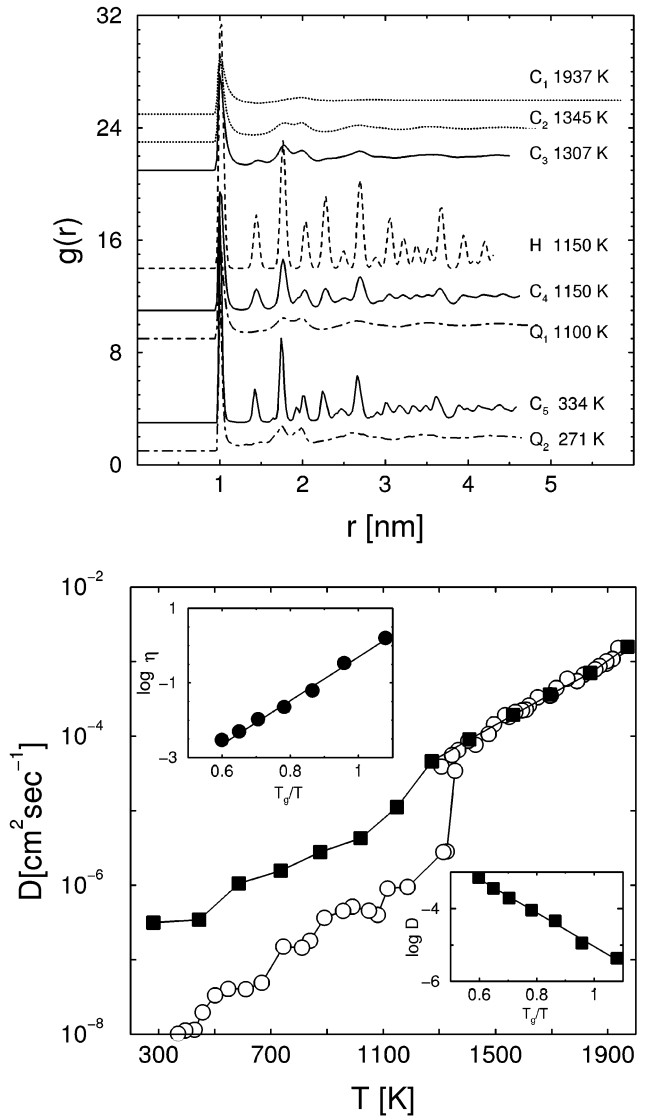

Figure 3. Top: evolution of the radial distribution function with temperature at $P = 3.5$ MPa. Cooling: C1−C2, normal and supercooled liquid; C3−C5, onset and development of crystallization. Quenching: Q1−Q2, development of the glass transition. Heating (of the perfect crystal from 300 K): H. Bottom: diffusion coefficient vs temperature in cooling (open circles) and quenching (full squares) cycles with $N = 864$ at $P = 3.5$ MPa. Inset: logarithm of viscosity η (in poise) and of the diffusion coefficient vs T_g/T.

The crystal is cooled to ≃300 K (see Figure 3) and then gradually heated through successive $\Delta T = 30$ K increases, up to the temperature at which melting occurs (see Figure 1). The "hysteresis" of the heating vs the cooling cycles is visible in Figures 1 and 2. Heating of a perfect fcc crystal of 864 Girifalco C_{60} molecules at $P = 3.5$ MPa is also performed from $T = 300$ K till the onset of melting; comparison at $T = 1150$ K with the $g(r)$ of the crystal previously attained through cooling, reveals the defective nature of the latter (see Figure 3).

Quenching of the liquid at $P = 3.5$ MPa is performed from an initial temperature equal to 1950 K, either by a sequence of $\Delta T = 150$ K temperature decrease steps or through a sudden $\Delta T = 1000$ K drop. Similarly to what is done in the cooling procedure, the temperature variations are imposed over 20 000 simulation steps, followed by 10 000 steps of free evolution. In both cases, a glassy phase is achieved. This is proved by (i) the V and H vs T patterns in Figure 2 showing a glass branch running above the crystallization line; (ii) the $g(r)$ curves which, as visible in Figure 3, exhibit, and maintain down to ≃300 K,

TABLE 1: Crystallization (c), Melting (m), and Glass (g) Transition Parameters (see text)[a]

P [MPa]	T_c [K]	ρ_c [nm^{-3}]	σ_{BH} [nm]	$\eta_c = \pi/6\rho_c\sigma_{BH}^3$
3.5	1307	1.124	0. 976	0.547
40	1464	1.130	0. 975	0.548
150	1880	1.138	0. 972	0.547
250	2200	1.150	0. 970	0.550
P [MPa]	T_m [K]	ρ_m [nm^{-3}]	σ_{BH} [nm]	$\eta_m = \pi/6\rho_m\sigma_{BH}^3$
3.5	1931	1.144	0. 9716	0.549
P [MPa]	T_g [K]	ρ_g [nm^{-3}]	σ_{BH} [nm]	$\eta_g = \pi/6\rho_g\sigma_{BH}^3$
3.5	1100	1.168	0.978	0.572
40	1170	1.177	0.977	0.575
150	1480	1.187	0.975	0.576
250	1700	1.190	0.973	0.574

[a] Melting data refer to the defective crystal with $N = 1000$.

the 2-fold structure of the second peak typical of the glass; (iii) the slope variations visible in the V, H, and D patterns (see Figures 2 and 3), also recorded in similar diagrams for the specific heat C_P, the thermal expansivity α, and the Wendt-Abraham ratio R of the first peak to the first minimum height in $g(r)$, (not shown for lack of space); (iv) the Arrhenius behavior of the shear viscosity η vs T, also shown in Figure 3, indicating that the glass formed is a "strong" one;[24] we note, in this instance, that the previously quoted orientational glass of C_{60} is similarly "strong".[1,2] The glass transition parameters are then obtained via the intersection of the two (extrapolated) branches of different slope in the V, H, C_P, and α vs T patterns (see ref 24): we estimate in this manner $T_g \simeq 1100$ K and $\rho_g \simeq 1.168$ nm^{-3} (see Table 1).

Glass transitions at higher pressures are also obtained via other quenching paths (one of which shown in Figure 1); we find, however, that the quenching rate has to be increased with respect to the $P = 3.5$ MPa case, when it was 1.5×10^{12} K/s. For instance, at $P = 250$ MPa, no glassy phase is obtained unless $\Delta T > 300$ K over 20 000 time steps. Glass temperatures and densities at different pressures are displayed in Table 1. The quenching rates adopted are much higher than those presently achievable in experiments (typically 10^8 K/s). We have, however, preliminary MD evidences[25] that in equimolar Girifalco C_{60}/C_{70} and C_{60}/C_{96} mixtures crystallization does not occur even under cooling rate 1 or 2 orders of magnitude lower than those adopted here; on the other hand, the C_{60}/C_{70} mixture, for instance, maintains liquid during the cooling procedure down to 1100 K, a temperature lower than that at which amorphization of pure C_{60} fullerite occurs[3] (see also note 7). These findings make it plausible that a glassy phase might experimentally be formed at least from mixed fullerene systems.

We now introduce an effective hard sphere diameter for the repulsive part of the C_{60} potential as follows. We first define a reference potential for $v(r)$ according to the well-known Weeks−Chandler−Andersen (WCA) prescription,[26] namely

$$v_{ref}(r) = \begin{cases} v(r) + \epsilon & r \le r_{min} \\ 0 & \text{if } r > r_{min} \end{cases} \qquad (2)$$

We then adopt the Barker and Henderson[27] expression for the effective hard-core diameter

$$\sigma_{BH} = \int_0^\infty \{1 - \exp[-\beta v_{ref}(r)]\}\, dr \qquad (3)$$

on its basis we define the packing fraction $\eta_c = \pi/6\rho_c\sigma_{BH}^3$, corresponding to the crystallization density ρ_c, and similarly η_m and η_g corresponding to the melting and glass transition densities, ρ_m and ρ_g, respectively. The result of such a simple scaling is remarkable: as visible in Table 1, the η_c and η_g sets of data group around two average values $\bar{\eta}_c = 0.548$ and $\bar{\eta}_g = 0.574$, with rms deviation as low as 1.09% and 1.56%, respectively, while η_m is practically equal to $\bar{\eta}_c$.

We now observe that $\bar{\eta}_g$ is quite close to the hard sphere glass transition value, $\eta_g^{HS} = 0.58$.[28] Effective packing fractions at vitrification have been reported by other authors (see, e.g., ref 29 and references therein), mostly for long-range Lennard-Jones-like potentials; their values approach, as in the present case, $\eta_g^{HS} = 0.58$, with however a considerably greater spread of values, interpreted as the result of different recipes for the effective diameter and for the determination of the glass transition temperature.[29] As far as the effective packing at melting $\eta_m = 0.549$ is concerned, this value is quite close to 0.545, corresponding to the packing fraction η_m^{HS} of hard spheres at melting.[30] Similarly, the crystallization packing $\bar{\eta}_c = 0.548$ turns out to be quite close to the minimum packing for incipient solidification as recorded in constant pressure MD simulation of hard spheres,[31] $\eta_c^{HS} = 0.55$, a value well beyond the packing at freezing $\eta_f^{HS} = 0.494$,[30] as determined via thermodynamic arguments.

It appears from these three sets of results that our model C_{60} quite closely follows a hard-sphere like behavior at the various transitions envisaged here.

The practically equal values of η_m and $\bar{\eta}_c$ also deserve comment. This result appears in fact correlated with the system's approach of two close instability thresholds, as documented below.

We first generalize the previous results on packing fractions, by imposing for any T the two equalities $\pi/6\rho_c(T)\sigma_{BH}^3 = \bar{\eta}_c = 0.548$ (with a similar equation for the melting) and $\pi/6\rho_g(T)\sigma_{BH}^3 = \bar{\eta}_g = 0.574$. We can determine on this basis (since $\sigma_{BH}(T)$ is known) the two functions $\rho_c(T)$ and $\rho_g(T)$ which we show in Figure 1. These two loci act of course as interpolation curves between the MD determined transition points and could in principle be used to determine transition temperatures and densities at other pressures, in terms of their intersections with specific cooling and quenching paths.

A further meaning of $\rho_c(T)$ transpires however from our results. It is in fact a finding of our simulations that when supercooling is pushed beyond this line the system invariably crystallizes. On the other hand, a state close to but on the left of the $\rho_c(T)$ line remains in the supercooled phase even over the longest MD run we could perform, namely 12 million simulation steps (60 ns). The characteristics of the $\rho_c(T)$ locus appear thus to approximate those of an instability boundary of the metastable region. It is worth recalling, in this instance, our recent Monte Carlo calculations[13] of the free energy of the Girifalco model at $T = 2100$ K, and reproduced in the inset of Figure 1. It appears that $\rho_c(2100\text{ K})$ coincides with the point where the free energy shows an inflection point associated with a sudden drop of the pressure of the simulation sample, i.e., a mechanical instability of the system. We surmise that something similar would be observed in the free energy branch generated by approaching the metastable region from the solid side. Since the interval separating the two branches in Figure 1 is quite narrow, it is conceivable that our simulation strategy is unable to discriminate between the densities at the crystallization and melting instabilities. We note that in constant pressure MD simulation of the Lennard-Jones potential, crystallization takes place much beyond the melting line, deeply inside the solid region.[32] On the other hand, we have independently verified

that states of the LJ system which are located inside the metastable fluid-solid region do not undergo crystallization even after 35 million MD time steps (≃180 ns).

The results we have presented appear in substantial agreement with recent mode coupling theory (MCT) predictions by Foffi et al.[18] of glass transitions in model protein solutions. For attractive hard-core Yukawa (HCY) potentials with inverse decay lengths z in the range 5−60 reciprocal particle diameters (through which protein−protein effective interaction is often mimicked), these authors find that the glass transition line is an almost vertical locus with a $T = \infty$ asymptote $\eta = \eta_g^{HS} = 0.58$. Now, as discussed in ref 17, the physical properties of the Girifalco model can reasonably well be reproduced by a HCY potential with $z \simeq 4$ (though with moderate differences in the phase diagram), close indeed to the lowest value investigated in ref 18. A qualitative but remarkable agreement thus emerges between the prediction of the two approaches as far as the occurrence of the glass transition and its location in the metastable fluid-solid region are concerned. Specific MCT calculations for the present model fullerene would be highly desirable at this stage, to compare the predicted structural arrest line with the present MD and $\rho_g(T)$ locus predictions of the glass line. Foffi et al.[18] also discuss "repulsive" and "attractive" glasses and find that at relatively low z (five, say) only the repulsive glass can be formed. According to our analysis, we identify the C_{60} "positional" glass as a repulsive one.

It appears, in conclusion, that effective hard core exclusion effects play a crucial role in determining the glass transition in systems with short-range strongly attractive potentials, like those currently used for the modelization of fullerenes, as well as of protein solutions, colloidal suspensions and colloid-polymer mixtures.[33] We surmise at this stage that the equation $\pi/6\rho_g(T)\sigma_{BH}^3 = \eta_g^{HS} = 0.58$ might hold to a high accuracy also for other model potentials, and hence it could be used for a qualitative but immediate prediction of the glass line through the determination of $\rho_g(T)$. A few MD quenching paths should be sufficient to assess such a first guess on a quantitative basis. A system worth applying to the present approach, possibly in parallel with MCT calculations, is a DLVO-like model of protein solutions, for which we have recently obtained accurate phase diagram predictions.[34] Calculations in this direction are under way.

Acknowledgment. The authors warmly thank Prof. J.-P. Hansen for discussions and suggestions. Useful correspondence with Prof. J. E. Fischer is also acknowledged. This work has been carried out in the framework of the Marie Curie Network on Dynamical Arrest of Soft Matter and Colloids, Contract No. MRTN−CT-2003−504712.

References and Notes

(1) Gugenberger, F.; Heid, R.; Meingast, C.; Adelmann, P.; Braun M.; Wuhl, M.; Haluska, M.; Kuzmany, H. *Phys. Rev. Lett.* **1992**, *69*, 1774.

(2) Matsuo, T.; Tsuo, T.; Suga, H.; David, W. I. F.; Ibberson, R. M.; Benrier, P.; Zahab, A.; Fabre, C.; Rassat, A.; Dworkin, A. *Solid State Comm.* **1992**, *83*, 711.

(3) Stetzer, M. R.; Heiney, P. A.; Fischer, J. E.; McGhie, A. R. *Phys. Rev. B* **1997**, *55*, 127.

(4) Xu, C.; Scuseria, G. E. *Phys. Rev. Lett.* **1994**, *72*, 669. Kim, S. C.; Tomanek, D. *Phys. Rev. Lett.* **1994**, *72*, 2418.

(5) Sundar, C. S.; Bharathi, A.; Hariharan, Y.; Janaki, J.; Sankara Sastri, V.; Radhakrishnan, T. *Solid State Comm.* **1992**, *84*, 823.

(6) Abramo, M. C.; Caccamo, C. *J. Chem. Phys.***1997**, *106*, 6475. Ruberto, R.; Abramo, M. C. *J. Chem. Phys.* **2004**, submitted for publication.

(7) Fullerite (crystalline C_{60}) heated at $T > 1200$ K, mostly transforms in amorphous carbon due to the disruption of the C_{60} cages (see ref 3). The latter, however, are predicted to be stable up to 3500−4000 K.[4] Solid state effects through molecule collision,[5] but also and alternatively residual impurities trapped in the crystalline matrix,[6] might trigger the cage instability.

(8) Cheng, A.; Klein, M. L.; Caccamo, C. *Phys. Rev. Lett.* **1993**, *71*, 1200.

(9) Hagen, M. H. J.; Meijer, E. J.; Mooij, G. C. A. M.; Frenkel, D.; Lekkerkerker H. N. W. *Nature* **1993**, *365*, 425.

(10) Ashcroft, N. W. *Nature* **1993**, *365*, 387.

(11) Mederos, L.; Navascues, G. N. *Phys. Rev. B* **1994**, *50*, 1301. Tau, M.; Parola, A.; Pini, D.; Reatto, L. *Phys. Rev. B* **1995**, *52*, 2644. Caccamo, C. *Phys. Rev B* **1995**, *51*, 3387.

(12) Hasegawa M.; Ohno, K. *J. Phys.: Cond. Matter*. **1997**, *9*, 3361; *J. Chem. Phys.* **1999**, *111*, 5955.

(13) Abramo, M. C.; Caccamo, C.; Costa, D.; Pellicane, G. *Europhys. Lett.* **2001**, *54*, 468.

(14) Costa, D.; Pellicane, G.; Abramo, M. C.; Caccamo, C. *J. Chem. Phys.* **2003**, *118*, 304.

(15) Girifalco, L. F. *J. Phys. Chem.* **1992**, *96*, 858.

(16) Alemany, M. M. G.; Rey, C.; Dieguez, O.; Gallego, L. J. *J. Chem. Phys.* **2000**, *112*, 10711.

(17) Hagen, M. H. J.; Frenkel, D. *J. Chem. Phys.* **1994**, *101*, 4093.

(18) Foffi, G.; McGullagh, G. D.; Lawlor, A.; Zaccarelli, E.; Dawson, K. A.; Sciortino, F.; Tartaglia, P.; Pini, D.; Stell, G. *Phys. Rev. E* **2002**, *65*, 031407. Dawson, K. A. *Curr. Opin. Colloid Interface Sci.* **2002**, *7*, 218.

(19) McPherson, A. *Preparation and Analysis of Protein Crystals*; Krieger: Malabar, FL, 1982.

(20) Muschol, M.; Rosenberger, F. *J. Chem. Phys.* **1997**, *107*, 1953.

(21) Eckert T.; Bartsch E. *Phys. Rev. Lett.* **2002**, *89*, 125701.

(22) Chen, S. H.; Chen, W. R.; Mallamace, F. *Science* **2003**, *300*, 619.

(23) Pham K. N.; Egelhaaf S. U.; Pusey P. N.; Poon W. C. K. *Phys. Rev. E* **2004**, *69*, 011503.

(24) Angell, C. A. *J. Non-Cryst. Solids* **1991**, *131*−*133*, 13.

(25) Abramo, M. C.; Caccamo, C.; Ruberto, R. Unpublished.

(26) Weeks, J. D.; Chandler, D.; Andersen, H. C. *J. Chem. Phys.* **1971**, *54*, 5237.

(27) Barker, J. A.; Henderson, D. *J. Chem. Phys.* **1967**, *47*, 2856.

(28) Woodcock, L. V. *Ann. N.Y. Acad. Sci.* **1981**, *37*, 274.

(29) Shumway, S. L.; Clarke, A. S.; Jonsson, H. *J. Chem. Phys.* **1995**, *102*, 1796.

(30) Alder, B. J.; Wainwright, T. E. *J. Chem. Phys.* **1959**, *31*, 459. Hoover, W. G.; Ree, F. H. *J. Chem. Phys.* **1968**, *49*, 3609.

(31) Gruhn, T.; Monson, P. A. *Phys. Rev. E* **2001**, *64*, 061703 and references therein.

(32) Nosè, S.; Yonezawa, F. *Solid State Comm.* **1985**, *56*, 1005; *J. Chem. Phys.* **1986**, *840*, 1803.

(33) Louis, A. A. *Philos. Trans. R. Soc. London A* **2001**, *359*, 939. Pham, K. N.; Egelhaaf, S. U.; Pusey, P. N.; Poon, W. C. K. *Phys. Rev. E* **2004**, *69*, 011503.

(34) Pellicane, G.; Costa, D.; Caccamo, C. *J. Phys. Chem. B* **2004**, *104*, 7538.